31 June 2002

Chemical Physics Letters 358 (2002) 284–289

CHEMICAL PHYSICS LETTERS

www.elsevier.com/locate/cplett

Quantum dissipative model for the collision induced ionization of I_2 impinging on a diamond surface

Gil Katz [a], Yehuda Zeiri [b], Ronnie Kosloff [a,*]

[a] *Department of Physical Chemistry and the Fritz Haber Research Center, The Hebrew University, Jerusalem 91904, Israel*
[b] *Department of Chemistry, Nuclear Research Center – Negev, P.O. Box 9001, Beer-Sheva 84190, Israel*

Received 21 January 2002; in final form 5 April 2002

Abstract

Negative ion production by impinging I_2 at hyperthermal energies on a diamond surface was modeled. A quantum time dependent nonadiabatic approach in Liouville space was used. The primary coordinate of the I_2 distance from the surface was modeled explicitly while the surface degrees of freedom were included implicitly using Lindblads semigroup formalism. The calculations were directed at determining the mechanism of the ion production. Two nonadiabatic crossing points were considered. By fitting the nonadiabatic parameters both crossing points could yield the increase in the ion production as a function of energy observed in the experiment. The mechanisms can be discerned by analyzing the relation between the kinetic energy distribution of the ions to that of the incident molecules. Ions are produced predominantly at a nonadiabatic crossing point located high in energy and close to the surface fit better the experimental observations. © 2002 Published by Elsevier Science B.V.

1. Introduction

Molecular ions such as I_2^- are produced when I_2 from the gas phase impinges on a diamond surface at hyper-thermal energy [1]. An exponential increase in ion production probability as a function of incident kinetic energy was measured experimentally. Saturation was reached at 10 eV with a total yield of 1%. Similar ion production behavior was observed for other systems [2–4]. The production of molecular ions starting with neutral molecules requires charge exchange between the molecule and the solid. The threshold energy of 3 eV observed in the experiment was related to the energy balance between the electron affinity of the I_2 (1 eV) and the work-function of diamond (4 eV).

Far from the surface the impinging neutral I_2 molecule is subject to a weak Van der Waals attractive force which becomes strong repulsion when the electron density of the molecule overlaps with that of the surface. This interaction of a molecule with the surface is described well by a Born–Mayer potential form [5,6]. The molecular ion I_2^- exhibits a long range Coulomb attraction to its image charge and a short range exponential repulsion. This repulsion is stronger than that of the neutral I_2 due to the additional electronic charge.

* Corresponding author. Fax: +972-2-6513742.
E-mail address: ronnie@grid.fh.huji.ac.il (R. Kosloff).

0009-2614/02/$ - see front matter © 2002 Published by Elsevier Science B.V.
PII: S0009-2614(02)00608-5

The energy difference at the asymptotic region determines the position of an outer crossing point between the ionic and neutral states. This crossing point is located at relatively large surface–particle distances, hence, the charge transfer process is in analogy to the harpooning phenomena known from gas phase collisions [7,8]. In addition, an inner crossing point at short molecule–surface separation should exist. This inner crossing is due to the stronger repulsion of the molecular ion compared to the neutral molecule. The energy range of the inner crossing point is high since it is located on the repulsive wall of both potentials. To facilitate comparison with previous studies [9–11] the same Morse potential form was adopted.

A theoretical framework explaining the experimental observations has to address the following mechanistic questions:

- Does the ion production occur in the inner or outer curve crossing point?
- Does the ion production occur mainly when the molecule approaches the surface or on its way out?
- What is the role of the internal degrees of freedom (molecular and solid degrees of freedom) in the charge transfer process?

A simple one-dimensional Landau–Zener–Stuckenberg (LZS) [12,13] model would predict that the ion production at the outer crossing point decreases as the incident kinetic energy increases. This contradicts the observed exponential increase of the negative ion production with kinetic energy. Ion production at the inner crossing point can show an exponential increase provided the inner crossing point energy is above the incident energy. The simple LZS picture above can be completely altered if internal degrees of freedom are considered. These include the I_2 vibration and rotation as well as the solid degrees of freedom, phonons and electron–hole pairs.

To examine some of these issues Bach and Gross [9] performed a multidimensional semiclassical nonadiabatic calculation for this system. Surface phonons and I_2 rotational degree of freedom [9,10] were included. The ion yield as a function of incident kinetic energy was found to be in good agreement with the experimental results. The discrepancy between these results and the 1-D LZS theory is explained by a large energy transfer from the I_2 to the solid which slows down the out going molecules. This in turn enhances the ion production at the outer crossing point. In this mechanism most of the ions are produced with a low mean kinetic energy, in contrast to the experimental observations [1].

A complete understanding of charge transfer events at solid surfaces requires a nonadiabatic quantum framework. The exponential growth of computational effort of quantum calculations with the number of degrees of freedom forces one to compromise either by reducing the number of degrees of freedom or to use semi-classical approximations.

A reduced dimensionality quantum description is based on the assumption that the encounter is dominated by a few degrees of freedom while the other coordinates are kept frozen. The validity of the assumption is dictated by the timescale of the encounter. A one-dimensional wavepacket calculation for this model was therefore performed [11] suggesting the possibility of ion formation at the inner crossing point. In this reduced 1D model, only the translation along the normal coordinate to the surface was included. The results showed, in contrast with experiment, a nonmonotonic ion production in the incident energy range of 4–9 eV. Such Stückelberg-like oscillations were interpreted as interferences of incoming and scattered parts of the wavepacket between the inner and outer crossing points. It can be expected that additional degrees of freedom would average out these oscillations.

The goal of the present study has been to establish a better understanding of the role of the surface degrees of freedom on the nonadiabatic ion production. The approach chosen was to partition the full system into a subsystem composed of the translational degree of freedom coupled to a bath composed of the various surface degrees of freedom. This approach was formulated in Liouville space where the subsystem is described by a density operator and the bath was implicitly included. Within this framework, the ion production mechanism was evaluated and compared to experiment.

2. Method and model

The equation of motion for the reduced density operator describing the system in Liouville space is given by

$$\frac{\partial\hat{\rho}}{\partial t} = -\frac{\mathrm{i}}{\hbar}\left[\hat{\mathbf{H}},\hat{\rho}\right] + \mathscr{L}_D(\hat{\rho}), \tag{2.1}$$

where the model Hamiltonian of the systems is

$$\hat{\mathbf{H}} = \begin{pmatrix} \mathbf{H}_{\mathrm{g}} & \mathbf{V}_{\mathrm{ge}} \\ \mathbf{V}_{\mathrm{eg}} & \mathbf{H}_{\mathrm{e}} \end{pmatrix}. \tag{2.2}$$

The diagonal elements are the ground and excited states Hamiltonians. The off diagonal elements represent the nonadiabatic coupling terms. The practical disadvantage of Liouville space is that the size of the state representation by a density operator is squared compared to a wavefunction representation, thus limiting the scope of systems that can be studied. The Hamiltonian of each state is given by

$$\hat{\mathbf{H}}_\alpha = \hat{\mathbf{T}}_\alpha + \hat{\mathbf{V}}_\alpha, \quad \alpha = g, e,$$

where $\hat{\mathbf{T}}_\alpha$ represents the kinetic energy operator in state α and $\hat{\mathbf{V}}_\alpha$ is the potential energy.

The model potential energy surfaces are chosen to be the same as in the wavepacket calculations [9,11]:

$$\begin{aligned} \hat{\mathbf{V}}_{\mathbf{g}}(z) &= D_g(\mathrm{e}^{-2\alpha_g(z-z_g)} - 2\mathrm{e}^{-\alpha_g(z-z_g)}) + S_g, \\ \hat{\mathbf{V}}_{\mathbf{e}}(z) &= D_e(\mathrm{e}^{-2\alpha_e(z-z_e)} - 2\mathrm{e}^{-\alpha_e(z-z_e)}) + S_e, \end{aligned} \tag{2.3}$$

where z is the surface molecule distance. The coupling term is given by

$$\hat{\mathbf{V}}_{\mathrm{ge}}(z) = D_{ge}\mathrm{e}^{-\alpha_{ge}z}, \tag{2.4}$$

where S_α are the energy shifts due to the difference between the work function and electron affinity ($s_g = 0$ and $s_e = 3$ eV). The potentials are presented in Fig. 1 and the parameters in Table 1.

The coupling of the primary system to the solid bath modes is generated by the dissipative superoperator $\mathscr{L}_D$. Within a Markovian approximation it is cast into Lindblads [14] semi-group form

$$\mathscr{L}_D(\hat{\rho}) = \sum_l \hat{\mathbf{F}}_l\hat{\rho}\hat{\mathbf{F}}_l^\dagger - \tfrac{1}{2}\{\hat{\mathbf{F}}_l^\dagger\hat{\mathbf{F}}_l,\hat{\rho}\}, \tag{2.5}$$

where $\hat{\mathbf{F}}_l$ are operators defined on the Hilbert space of the primary system. These equations allow a consistent study of a variety of dissipative models by choosing the appropriate operator $\hat{\mathbf{F}}_l$ to describe a particular system-bath encounter. The Liouville von Neumann equation was solved numerically by the Newtonian method [15,16]. In the present study three possible channels of system–surface interaction are considered. The first represents energy transfer to the surface phonons and is given by

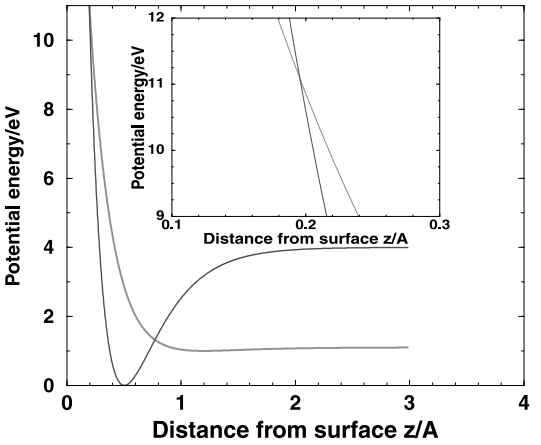

Fig. 1. The model potentials employed in the calculations. At large distances the upper curve represents the molecular-ion–surface potential and the lower curve the molecular-surface potential. Notice the inner and outer crossing points. (Parameters are described in Table 1.)

Table 1
The parameters of the potentials used for the wavepacket and Liouville calculations (the figures in the brackets are the parameters used in [9])

Potential	D (eV)	α ($\mathrm{\AA}^{-1}$)	z_{eg} ($\mathrm{\AA}$)
V_g	0.1	2.4 (3.)	1.2 (1.)
V_e	4.	3.18 (3.)	0.5
V_{ge} (wavepacket)	0.054 (.2)	3.4 (2.)	–
V_{ge}^* (Liouville)	0.049	3.77	–
$\hat{F}$	F ($\mathrm{fs}^{-1/2}$)	γ ($\mathrm{\AA}^{-1}$)	η ($\mathrm{\AA}^{-1}$ $\mathrm{fs}^{-1/2}$)
$\hat{F}_p$	0.00009	.9	−.0005
$\hat{F}_s$	0.112	1.5	–
$\hat{F}_q$	0.336	2.5	–

$$\hat{\mathbf{F}}_p(z) = \begin{pmatrix} F_p^0 e^{-\gamma_p z} & 0 \\ 0 & F_p^0 e^{-2\gamma_p z} - \frac{\eta_p}{z - z_p} \end{pmatrix}, \tag{2.6}$$

where F_p^0 is determined by the time scale of energy transfer to phonons ($\tau \sim 1$ ps) and is proportional to $\sqrt{1/\tau}$. The rate of decay as a function of particle–surface distance is given by γ_p. The additional Born–Mayer term represents energy transfer to phonons induced by the image charge of the ionic state.

Another channel of energy dissipation is a production of a compression wave or shock wave generation in the solid [17,18]. The operator $\hat{\mathbf{F}}_s$ modeling this phenomena has the form

$$\hat{\mathbf{F}}_s = F_s^0 e^{-\gamma_s z} \otimes \begin{pmatrix} 1 & 0 \\ 0 & 1 \end{pmatrix}, \tag{2.7}$$

where F_s^0 is determined by the time scale of energy transfer through shock wave generation ($\sim$10 fs). The compression wave generation decays exponentially with the distance from the surface represented by the parameter γ_s. Both the phonons and shock wave generation dissipate the energy of the collision but do not induce direct nonadiabatic transfer.

A third dissipative channel involves electronic quenching. The electronic quenching operator is modeled by

$$\hat{\mathbf{F}}_Q(z) = F_Q^0 e^{-\gamma_Q z} \otimes \begin{pmatrix} 0 & 1 \\ 0 & 0 \end{pmatrix}, \tag{2.8}$$

where F_Q^0 is related to the typical electronic quenching time scale, $\sim$3 fs.

This dissipative term describes a nonadiabatic transition from the higher covalent diabatic potential surface to a lower ionic surface. Quenching is assumed to be efficient only at small surface–particle separations. The reverse transitions are activated and therefore are not included because of the required large energy jump. The probability of obtaining this energy from the cold solid surface is negligible. The result is a nonsymmetric dissipative operator.

3. Results and discussion

The approach chosen to reveal the dominating mechanism of ion production was to isolate the contribution of each individual phenomena. To single out the crossing point that dominates charge transfer, a wavepacket calculation was performed with the nonadiabatic coupling turned off at the inner or outer turning points. This was done by using a Gaussian nonadiabatic coupling potential centered at either the inner or outer crossing points. The coupling parameters matched at this position the value of the nonadiabatic term with parameters from Table 1. The influence of dissipation was studied using the semi-group approach with different dissipative operating mechanisms. This was followed by a calculation which included both the electronic quenching and the phononic and shock wave dissipation mechanism. A range of incident kinetic energies of the incoming I_2 molecule was examined. The scattering process was simulated for a duration of 100 fs. The parameters of the model are summarized in Table 1. Adjustments to the nonadiabatic coupling were made to fit the experimental maximum ion production at high incident kinetic energy. The ionization probabilities were calculated from the wavepacket partial norm of the excited state at the final time for $z \geqslant 2$ Å.

Fig. 2 shows a comparison between three wavepacket calculations performed with nonadiabatic coupling operating at different regions of the potential energy surfaces. It is clear from Fig. 2

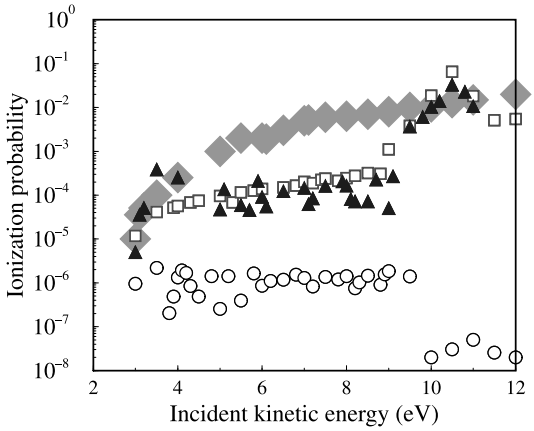

Fig. 2. Ionization probability as a function of incident kinetic energy for wavepacket calculations. Experimental results (diamonds), inner and outer crossing points operative (triangles pointing up), coupling only at the outer crossing point (circles), coupling only at the inner crossing point (squares).

that the dominating mechanism of ion production is located at the inner crossing point. The outer crossing point contributes to Stückelberg-like oscillations in the ion yield. This can be observed by comparing the calculation with both crossing points contributing to the one where the coupling at the outer crossing point is turned off. When only the outer crossing point is operating the ion yield is very low with negligible energy dependence.

Fig. 3 repeats the wavepacket calculations with the parameters of [9]. For this case the inner crossing is located high at 16 eV and the nonadiabatic coupling is large and decays slowly. The figure shows that the ion production is dominated at the outer crossing point. When only the inner crossing point is operative the ion production shows a typical tunneling exponential increase with kinetic energy (see Fig. 4).

Comparing the ion production in the different dissipative mechanisms to the experiments leads to the following observations: Up to energies of ~5 eV all dissipative mechanisms show a similar exponential increase of ion yield, with a yield higher than the equivalent wavepacket calculation. Above this energy only the electronic quenching mechanism leads to further monotonic increase in ion yield.

The calculated ion kinetic energy distribution for the electronic quenching case is shown in Fig. 5,

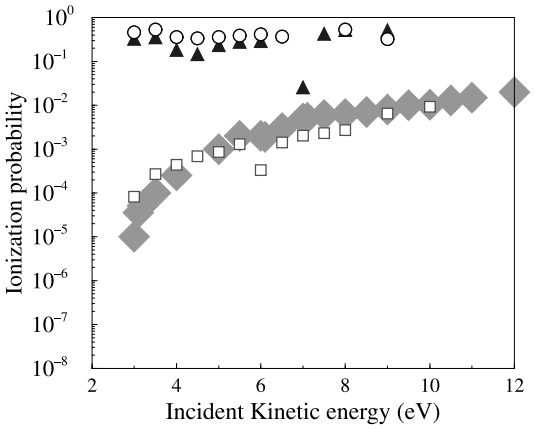

Fig. 3. Ionization probability as a function of incident kinetic energy for wavepacket calculations with parameters of [9]. Experimental results (diamonds), inner and outer crossing points operative (triangles pointing up), coupling only at the outer crossing point (circles), coupling only at the inner crossing point (squares).

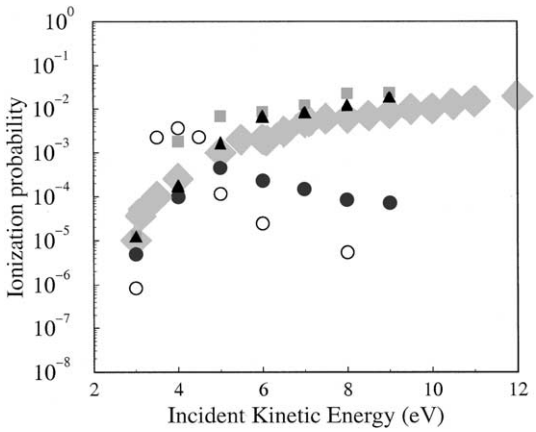

Fig. 4. Ionization probability as a function of incident kinetic energy for density operator calculations. Experimental results (diamonds). Dissipation by electronic quenching, shock-wave production and phonon generation (triangles pointing up). Electronic quenching only (squares). Shock-waves and phonons only (full circles). Calculations using the parameters of [9] and phonon dissipation only (empty circles).

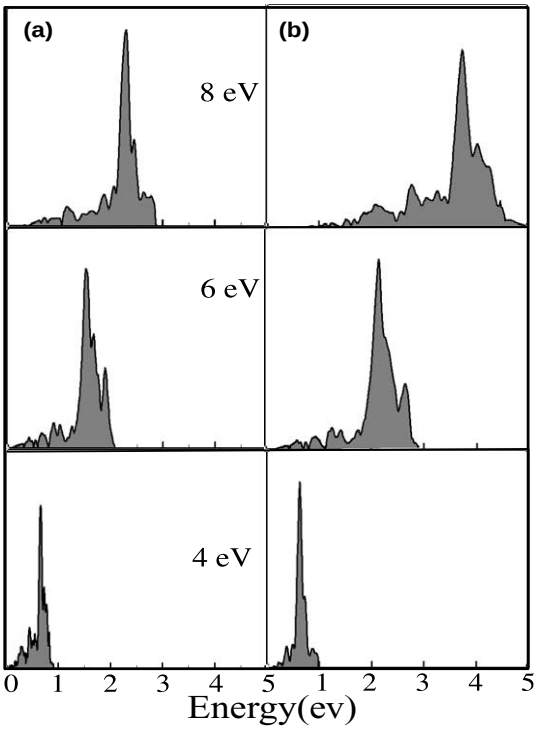

Fig. 5. Kinetic energy distribution of the outgoing molecular ions as a function of incident kinetic energy of the neutral incoming molecules. Panel a: phononic dissipation; panel b: electronic quenching.

panel b. One observes that the distribution reaches a threshold with a tail to lower energies. The threshold is found at the maximum allowed energy, determined by subtracting the endothermicity of ion production from the incident kinetic energy. Energy loss to the solid causes the tail toward lower ion kinetic energy. The mean kinetic energy of the ions is almost linearly proportional to the incident kinetic energy of the incoming molecules. A similar behavior of the threshold and mean kinetic energy is found also in the experimental data [1]. Fig. 5, panel a shows the kinetic energy distribution for coupling only at the outer crossing point with phononic dissipation. The threshold does not reach the maximum allowed value and the mean ion kinetic energy is sub-linear with the incident energy. This behavior can be rationalized by the fact that for this model the ion production is hindered by high outgoing kinetic energy.

4. Conclusions

In the present study the mechanism of ion production at the inner crossing point enhanced by electronic quenching fits best the experimental observations. The main argument is one of energy balance. An outgoing molecular ion found at the asymptote must have at least $\sim$3 eV when it passes the outer crossing point. The probability to jump from the neutral to ionic curve at this crossing position should follow LZS theory and decrease with energy. If the ion does not have sufficient energy to escape it will oscillate in the ionic state and eventually escape as a neutral by a back transfer of charge, decreasing therefore the ionic production. Enhancement of ion production at the inner crossing point can be attributed to its proximity to the turning point which is a result of the steepness of the repulsive wall. Moreover the nonadiabatic coupling interaction also maximizes at this location. Energy transfer to phonons is negligible on the time scale of the collision. Kinetic energy loss to the surface through the dominant shock-wave and minor phonon generation mostly suppresses the ion production. Finally electronic quenching increases significantly the ion production above energies of $\sim$4 eV, and it causes the low energy tail in the final kinetic energy distribution.

Acknowledgements

This research was supported by the German–Israel Foundation (GIF). We want to thank Aviv Amirav for helpful discussions. The Fritz Haber Research Center is supported by the Minerva Gesellschaft für die Forschung, GmbH München, Germany.

References

[1] A. Danon, A. Amirav, Phys. Rev. Lett. 61 (1998) 2961.
[2] A. Danon, A. Amirav, Israel J. Chem. 29 (1989) 443.
[3] A. Danon, A. Amirav, Phys. Rev. Lett. 65 (1990) 2038.
[4] A. Danon, A. Amirav, J. Phys. Chem. 93 (1989) 5549.
[5] K.T. Tang, J.P. Toennies, J. Chem. Phys. 80 (1984) 3726.
[6] G. Ihm, M.W. Cole, F. Toigo, G. Scoles, J. Chem. Phys. 87 (1987) 3995.
[7] R.A.J. Ogg, M. Polanyi, Trans. Faraday Soc. 31 (1935) 604.
[8] M.G. Evans, M. Polanyi, Trans. Faraday Soc. 34 (1938) 11.
[9] C. Bach, A. Gross, Faraday Discuss. Chem. Soc. 117 (2001) 99.
[10] C. Bach, A. Gross, J. Chem. Phys. 114 (2001) 6396.
[11] R. Kosloff, Faraday Discuss. Chem. Soc. 117 (2001) 172.
[12] C. Zener, Proc. R. Soc. A 137 (1932) 696.
[13] L.D. Landau, E.M. Lifshitz, Quantum Mechanics, Non Relativistic Theory, Pergamon, London, 1958.
[14] G. Lindblad, Commun. Math. Phys. 48 (1976) 119.
[15] P. Saalfrank, R. Baer, R. Kosloff, Chem. Phys. Lett. 230 (1994) 463.
[16] W. Huisinga, L. Pesce, R. Kosloff, P. Saalfrank, J. Chem. Phys. 110 (1999) 5538.
[17] E. Kolodney, A. Amirav, R. Elber, R.B. Gerber, Chem. Phys. Lett. 111 (1984) 636.
[18] E. Kolodney, A. Amirav, R. Elber, R.B. Gerber, Chem. Phys. Lett. 113 (1984) 303.